



Ocean dynamics shapes the structure and timing of Atlantic equatorial modes

Marta Martín-Rey, Irene Polo, Belén Rodríguez-Fonseca, Alban Lazar, Teresa Losada

► To cite this version:

Marta Martín-Rey, Irene Polo, Belén Rodríguez-Fonseca, Alban Lazar, Teresa Losada. Ocean dynamics shapes the structure and timing of Atlantic equatorial modes. *Journal of Geophysical Research. Oceans*, 2019, 124 (11), pp.7529-7544. 10.1029/2019JC015030 . hal-02408951

HAL Id: hal-02408951

<https://hal.sorbonne-universite.fr/hal-02408951>

Submitted on 13 Dec 2019

HAL is a multi-disciplinary open access archive for the deposit and dissemination of scientific research documents, whether they are published or not. The documents may come from teaching and research institutions in France or abroad, or from public or private research centers.

L'archive ouverte pluridisciplinaire **HAL**, est destinée au dépôt et à la diffusion de documents scientifiques de niveau recherche, publiés ou non, émanant des établissements d'enseignement et de recherche français ou étrangers, des laboratoires publics ou privés.

Ocean dynamics shapes the structure and timing of Atlantic Equatorial Modes

Marta Martín-Rey ^{(1-2)*}, Irene Polo ⁽³⁾, Belén Rodríguez-Fonseca ⁽³⁻⁴⁾, Alban Lazar ⁽²⁾
and Teresa Losada ⁽³⁾

(1) UMR5318 CECI CNRS-CERFACS, Toulouse, France

(2) Laboratoire d’Oceanographie et du Climat: Expérimentation et Approches Numériques (LOCEAN), Université Pierre et Marie Curie (UPMC), Universités Sorbonnes, Paris, France

(3) Departamento de Física de la Tierra y Astrofísica, Facultad de C.C. Físicas, Universidad Complutense de Madrid (UCM), Madrid, Spain.

(4) Instituto de Geociencias, Consejo Superior de Investigaciones Científicas, Universidad Complutense de Madrid, Madrid, Spain.

*Current corresponding author address: Marta Martín del Rey. Institut de Ciències del Mar (ICM-CSIC), Passeig Marítim de la Barceloneta, 37-49, 08003 Barcelona, Spain.
Email: mmartin@icm.csic.es

Key points

- Ocean waves determine the distinct timing of the Equatorial Modes under negative AMV phases
- Equatorial Kelvin waves favour the development of Equatorial Modes, while a remotely-excited Rossby wave damps the equatorial SST anomalies
- Diverse ocean dynamics activated during negative AMV phases modulate the development of different Equatorial Modes

Abstract

A recent study has brought to light the co-existence of two distinct Atlantic Equatorial Modes during negative phases of the Atlantic Multidecadal Variability: the Atlantic Niño and Horse-Shoe (HS) mode. Nevertheless, the associated air-sea interactions for HS mode have not been explored so far and the prevailing dynamic view of the Atlantic Niño has been questioned. Here, using forced ocean model simulations, we find that for both modes, ocean dynamics is essential to explain the equatorial SST variations, while air-sea fluxes control the off-equatorial SST anomalies. Moreover, we demonstrate the key role played by ocean waves in shaping their distinct structure and timing. For the positive phase of both Atlantic Niño and HS, anomalous westerly winds trigger a set of equatorial downwelling Kelvin waves (KW) during spring-summer. These dKWs deepen the thermocline, favouring the equatorial warming through vertical diffusion and horizontal advection. Remarkably, for the HS, an anomalous north-equatorial wind stress curl

excites an upwelling Rossby wave (RW), which propagates westward and is reflected at the western boundary becoming an equatorial upwelling KW. The uKW propagates to the east, activating the thermocline feedbacks responsible to cool the sea surface during summer months. This RW-reflected mechanism acts as a negative feedback causing the early termination of the HS mode. Our results provide an improvement in the understanding of the TAV modes and emphasize the importance of ocean wave activity to modulate the equatorial SST variability. These findings could be very useful to improve the prediction of the Equatorial Modes.

Plain Language Summary

A recent study has found how the inter-annual variations of sea surface temperature (SST) in the tropical Atlantic, are organized in two different equatorial modes during negative phases of the Atlantic Multidecadal Variability. These modes, which illustrate a particular and distinct spatial structure, are denoted as Atlantic Niño and Horse-Shoe mode. Here we show that, for both patterns, ocean dynamics is key to generate equatorial SSTs, while the off-equatorial SST anomalies are mainly explained by thermodynamic processes (heat fluxes exchanges). Outstandingly, we demonstrate that ocean waves have a substantial impact in the development and decay of Atlantic Niño and Horse-Shoe modes, shaping their distinct spatial configuration and timing. Our results bring to light the importance of ocean wave activity to explain the modulation of the equatorial Atlantic SST variability, which could be relevant to improve its predictability and associated climatic impacts.

1. Introduction

The Atlantic Niño, also named as Equatorial Mode, is an air-sea coupled mode that dominates the inter-annual tropical Atlantic variability (TAV) during boreal summer (Zebiak 1993; Lübbecke et al. 2018). Its positive phase is characterized by a relaxation of climatological trades and an anomalous warming in the eastern equatorial Atlantic. The Atlantic Niño significantly influences the precipitation regime of remote and adjacent areas (Kucharski et al. 2008; Polo et al. 2008a; Losada et al. 2012a; 2012b), causing important socio-economic impacts (Rodríguez-Fonseca et al. 2015; Lübbecke et al. 2018). Thus, a complete understanding of the role of atmospheric forcings, as well as the associated air-sea mechanisms and ocean dynamics, is necessary to anticipate these phenomena. Remarkably, a recent study by Martín-Rey et al. (2018) has demonstrated a modulation of the tropical Atlantic variability (TAV) modes under different phases of the Atlantic Multidecadal Variability (AMV, Knight et al. (2006)). In particular, these authors have brought to light a new overlooked equatorial mode, the so-called Horse-Shoe (HS) mode, which coexists with the Atlantic Niño during negative AMV phases. The HS pattern emerges as the second TAV mode during boreal summer, and is forced by an ENSO event from previous winter (Martín-Rey et al. 2018). The positive phase of HS is referred, hereinafter, to an anomalous equatorial warming surrounded by negative SST anomalies in north and south-western TA (Figure S1b).

87 The co-existence of Atlantic Niño and HS during negative AMV phases, is understood in
88 terms of a distinct contribution of the Subtropical Highs acting under shallow mean
89 thermocline conditions in the eastern equatorial Atlantic. This could imply a more
90 effective Bjerknes feedback (Bjerknes 1969), enhancing the equatorial SST variability
91 and making the TA more receptive to external forcings (Martín-Rey et al. 2018). The
92 emergence of different configurations of the Equatorial Mode is a key element to
93 understand the multidecadal changes experienced by TAV, since different Atlantic Niño
94 structures have been associated with a modification of its climate impacts (Losada et al.
95 2012b; Martín-Rey et al. 2014; Losada and Rodríguez-Fonseca 2016; Martín-Rey et al.
96 2018).

97
98 Recent studies have questioned the air-sea interactions and ocean mechanisms
99 responsible to develop the Atlantic Niño, becoming a controversial topic (Lübbecke et al.
100 2010; Brandt et al. 2011; Richter et al. 2013; Nnamchi et al. 2015, 2016; Jouanno et al.
101 2017; Planton et al. 2018). Traditionally, it has been established that a relaxation of south-
102 easterly trades related to an anomalous weakening of the South Atlantic Anticyclone
103 (SAA), leads the generation of the Atlantic Niño (Polo et al. 2008a; Lübbecke et al. 2010).
104 These anomalous winds activate the dynamical Bjerknes feedback (Bjerknes 1969),
105 which drives the development of Atlantic Niño pattern and makes it self-sustaining
106 (Keenlyside and Latif 2007; Lübbecke and McPhaden 2013; Polo et al. 2015a). The
107 Bjerknes mechanism implies the propagation of equatorial Kelvin waves (Keenlyside and
108 Latif 2007), which can contribute to generate equatorial SST anomalies (Carton and
109 Huang 1994; Hormann and Brandt 2009; Lübbecke et al. 2010; Planton et al. 2018). The
110 ocean responds to the surface wind forcing through an adjustment of the vertical
111 stratification, giving rise to baroclinic (mode) Kelvin (KW) and Rossby waves (RW)
112 (Illig et al. 2004). These baroclinic ocean modes are characterized by opposite-sign
113 anomalies of sea surface height and thermocline depth and propagate with different phase
114 speeds (high-order modes are the slower ones, Illig et al. (2004)). Illig et al. (2004) and
115 Polo et al. (2008b) proposed an active contribution of the three first baroclinic modes
116 (ranging from 0.9 to 2.8 m/s and 0.28 to 0.89 m/s for KW and RW respectively) in the
117 equatorial Atlantic variability. In particular, these authors reported the existence of ocean
118 wave activity in the development and decay of the Atlantic Niño (Polo et al. 2008a;
119 Lübbecke et al. 2010). Nevertheless, other studies showed pronounced discrepancies
120 between events (Carton and Huang 1994; Hormann and Brandt 2009). Recent findings
121 have suggested alternative mechanisms to generate the equatorial Atlantic SST
122 variability, as equatorward advection of north tropical Atlantic subsurface temperature
123 anomalies (Richter et al. 2013) or equatorial deep jets (Brandt et al. 2011). Moreover,
124 Nnamchi et al. (2015); (2016) have argued that thermodynamic processes are enough to
125 create equatorial ocean variability, opening the debate about the dynamic prevailing view
126 of the Atlantic Niño.

127
128 In this context, the present study aims to clarify the air-sea interactions and oceanic
129 mechanisms responsible to generate the equatorial Atlantic variability. The co-existence
130 of two distinct Equatorial Modes (Atlantic Niño and HS) during negative AMV phases,

provides a favourable framework to investigate in detail the processes underlying their development and decay. In particular, we will determine for the first time the air-sea mechanisms and wave activity associated with the recently discovered HS mode, and compare it with the Atlantic Niño pattern. For this purpose, an inter-annual simulation with a forced ocean model has been performed and analysed for a negative AMV period (1968-1995). Although coupled models suffer from strong and persistent biases in the TA (Richter and Xie 2008; Richter et al. 2014; Wang et al. 2014), sensitivity experiments correcting the surface winds reveal a considerably improvement in the simulation of the TA climate (Goubanova et al. 2018). Thus, ocean simulations forced with observed atmospheric fields, represent a good alternative to explore the TAV. Moreover, the ocean model used in the present study, is able to compute interactively a closed heat budget in the tropical Atlantic mixed layer. This allows us to investigate the different air-sea processes and feedbacks involved in the development of the HS and Atlantic Niño modes.

The paper is organized as follows. The model description and methodology used are detailed in Section 2. The results are explained in Section 3: the simulated TAV is described in Section 3.1; Section 3.2 assesses the wave activity associated with the development of the Atlantic Niño and HS patterns, while a closed heat budget analysis is carried out in Section 3.3. Finally, the main findings and discussion are presented in Section 4.

2. Data and Methods

2.1 Model description

A tropical Atlantic configuration of the ocean NEMO model (Madec 2008), named ATL TROP025 (Faye et al. 2015), has been used. The horizontal resolution is $\frac{1}{4}^\circ$ with a tripolar grid and 46 z-levels. The ocean model has been forced by inter-annual air-sea fluxes from the DRAKKAR forcing set, version DFS4.4 (Brodeau et al. 2010), for the period 1958-2011. This inter-annual simulation, hereinafter INTER simulation, starts from stable conditions taken from a stabilized climatological run. Nevertheless, to avoid the initial shock of the model, the first two years of the experiment have been dismissed. Thus, INTER covers the period 1960-2011 and reproduces quite well the TA seasonal cycle and variance, although standard warm SST biases appear in the upwelling regions (up to 1.5°C , Figure 1a). A cold bias is also shown in the western equatorial Atlantic (Figure 1a), accompanied by a shallower mixed layer (not shown), reduced sea surface height (SSH, Figure 1b) and a reduction of the east-west thermocline slope (Figure 1c).

Observations from HadISST (Rayner et al. 2003) and version 2.2.4 of SODA reanalysis (Giese and Ray 2011) have been used to validate the modelled SST, thermocline depth and SSH. The simulation of mixed layer depth (not shown) has been evaluated using the observational climatology from de Boyer Montegut et al. (2004). Despite its persistent biases, the tropical Atlantic variability is quite well simulated by INTER simulation (Figure 2 and Figure S1).

The modelled variables used throughout the manuscript are: wind stress, SSH, SST and the depth of the isotherm of 18°C as a proxy of thermocline depth (D18). In this study, we consider D18 instead of the commonly used isotherm of 20°C, to assure a complete representation of the tropical Atlantic subsurface, including the equatorial and coastal upwellings. According to the results from Martín-Rey et al. (2018), the negative AMV period 1968-1995 is analysed in the present study.

2.2 Methods

Inter-annual anomalies were computed by subtracting the climatological seasonal cycle of the whole period (1960-2011). This calculation has been done for each 4-month season, from JFMA to DJFM for the space-time fields. The amplitude interannual SST anomalies, and thus the interannual modes, are strongly influenced by low-frequency variability associated with natural decadal patterns (i.e: Atlantic Multidecadal Variability; Pacific Decadal variability) or the anthropogenic forcing (Tokinaga and Xie 2011; Martín-Rey et al. 2018). These low-frequency signals can modulate the amplitude and structure of the SST anomalies in the tropical Atlantic, giving rise to the decadal modulation of the interannual modes (Losada and Rodríguez-Fonseca 2016; Martín-Rey et al. 2018). However, in the present study we focus on the interannual variability modes that emerge during a negative AMV period. In order to isolate the inter-annual variability and subtract the low-frequency signal and the global warming trend, a 7-year cut-off Butterworth filter (Butterworth 1930) has been applied to the seasonal (4-month) anomalies. Focusing on Atl3 index, as a proxy for the equatorial SST variability, we have verified that the Butterworth filter used here has a very satisfactory response, retaining only those frequencies between 2-7 years (not shown). Therefore, the Atl3 index does not contain GW trend or the low-frequencies associated with natural decadal variability, which exhibit a strong decadal peak (not shown). To better visualize the wave propagation, a band-pass Butterworth filter that retains the frequencies between 60-days and 540-days, has been applied to the 5-day mean data of wind stress and SSH anomalies.

We computed the dominant modes of TA SST variability using the principal component analysis (PCA). PCA has been applied to the interannually filtered boreal summer (June-July-August-September) SST anomalies in the tropical Atlantic region limited by the model boundaries: [58°W-18°E, 31°S-30°N]. PCA technique provides the Empirical orthogonal functions (EOFs) and associated time series (principal components, PC), together with the percentage of explained variance (von Storch and Zwiers 2001). The independence of the modes has been evaluated using the North criterion (North et al. 1982).

Most of the results of the present study are based on lagged regression maps. Seasonal anomalies, for each 4-month season from JFMA to DJFM (shifting one month in each consecutive season) are regressed onto the boreal summer (JJAS) PC of the Atlantic Niño and HS mode. Similarly, 5-day SSH and wind stress anomalies, for each 5-day time step from January to December, are regressed onto the Atlantic Niño and HS time series (PC). Two transects along 2°N-4°N and along the equator, have been selected for the time-

longitude hövmoller diagrams. Statistical significance is assessed according to a t-test with 95% confidence level.

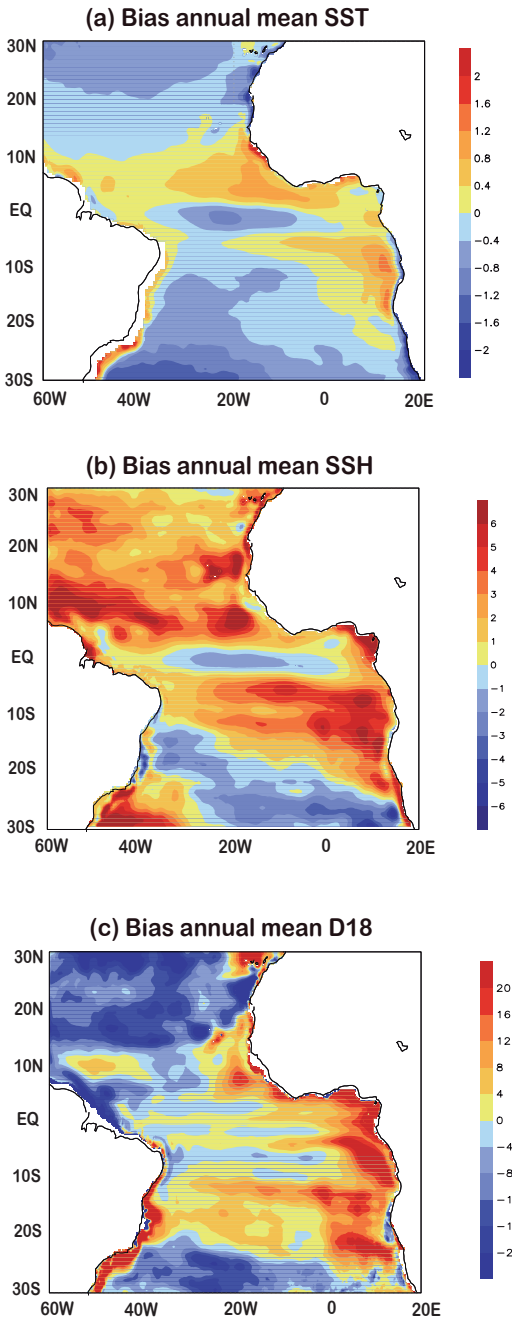


Figure 1. Validation of INTER simulation. Bias of the annual SST(a), SSH (b) and thermocline depth (D18, c) of INTER simulation with respect to SODA reanalysis for the period the period 1960-2008.

2.3 Heat Budget analysis

To determine the air-sea processes underlying the development of the HS and Atlantic Niño mode, a closed heat budget analysis has been computed interactively by NEMO-ATLTROP025 model in the TA mixed layer (ML). The temporal variations of the ML

temperature are given by a balance of atmospheric (a) and oceanic terms (b-c), according to the equation (Faye et al. 2015; Polo et al. 2015a):

$$\partial_t \langle T \rangle = \underbrace{\frac{Q_s (1-F_{z=h}) + Q^*}{\rho C_p h}}_a - \underbrace{\langle \overline{U_h} \cdot \overline{\partial_h T} \rangle + \langle D_l(T) \rangle}_b - \underbrace{\langle w \cdot \partial_z T \rangle - \frac{1}{h} (K_z \partial_z T)_{z=h}}_c + res \quad [1]$$

with $\langle \cdot \rangle = \frac{1}{h} \int_{-h}^0 \cdot dz$. The brackets denote the vertical integration over the ML with T and h representing the temperature and depth of the ML respectively; $\overline{U_h}$ and w are the horizontal and vertical currents; $D_l(T)$ is the lateral diffusion operator and K_z the vertical mixing coefficient. The *res* term has been calculated as a residual and is associated with the entrainment in the base of the ML. Thus, *res* term represents the upwelling of deep cold waters into the mixed layer. The net heat flux, Q_{net} , is divided in solar (Q_s) and non-solar (Q^*) components, and $F_{z=h}$ is the exponential function that describes the fraction of shortwave fluxes penetrating in the ML. Finally, ρ is the seawater density and C_p is the seawater specific heat capacity coefficient.

The oceanic component includes horizontal (b, zonal and meridional advection and lateral diffusion) and vertical processes (c, turbulent mixing or vertical diffusion, vertical advection and entrainment). All terms from equation [1] are provided as outputs by INTER simulation for the period 1968-1995. The calculation of seasonal (4-month) anomalies for the different heat budget terms has been performed in a similar way than for the rest of the atmospheric and oceanic variables. This approach is a useful method to understand the oceanic processes related to the formation of ENSO (Vialard et al. 2001) and Atlantic Niño (Polo et al. 2015a).

3. Results

3.1 Simulated boreal summer tropical Atlantic variability

INTER simulation reproduces the observational results of Martín-Rey et al. (2018), hereinafter MR18, for the 1968-1995 period (Figure 2a-b). The Atlantic Niño and HS emerge as the first two leading modes, exhibiting significant equatorial SST anomalies. It is worth mentioning that the commonly used Atl3 index [20°W-0°, 3°N-3°S], previously filtered, is a good indicator for both phenomena (Figure S1d). However, during negative AMV periods, when both modes co-exist, we also need an additional index referred to the western-equatorial Atlantic, WEQ [50°W-30°W, 3°N-3°S], to determine which equatorial mode is emerging in the tropical Atlantic basin. For Atlantic Niño pattern, same sign SST anomalies are found in WEQ and Atl3 (stars, Figure S1d), while opposite-sign ones are exhibited during the HS mode (dots, Figure S1d). Notice that there are some years in which mixed events occurred (i.e: 1971, 1973 or 1986). In those cases, the resultant spatial pattern will fit better with the Atlantic Niño or HS mode depending on the combination of the loadings of each PC (Figure 2c). The observed

explained variance and inter-annual variability are also well captured by the model (Figure 2a-c and Figure S1a-b). This result confirms the important finding of MR18: the existence of two distinct Equatorial Modes during negative AMV phases.

The basin-wide Atlantic Niño pattern described in MR18 for negative AMV phases is well reproduced by INTER (Figure 2a and Figure S1a). INTER also simulates the general reduction of tropical trades during previous winter-spring (Figure 5b,f), caused by a simultaneous weakening of the Subtropical Highs (Martín-Rey et al. 2018). Interestingly, The Atlantic Niño during negative AMV exhibits an early development, starting from previous fall-winter (Figure 2d) and it is characterized by a westward extension of its equatorial warm tongue (Figure 2a), compared with the canonical Atlantic Niño (see Figure 5 in (Losada and Rodríguez-Fonseca 2016; Martín-Rey et al. 2018). The reduced equatorial winds are accompanied by an elevation of the SSH in the eastern equatorial Atlantic (purple contours, Figure 2a), in agreement with previous studies (Polo et al. 2008a; Lübbecke et al. 2010).

The emergence of the overlooked HS pattern during negative AMV phases is well captured by INTER simulation (Figure 2b and Figure S1b). Moreover, the modelled evolution of HS agrees with MR18: intensified northern and southern trades during winter-spring and anomalous equatorial westerlies (Figure 6b,f), related to the ENSO-induced atmospheric forcing (Martín-Rey et al. 2018). The weakened surface winds along the equatorial band originate a zonal SSH gradient with positive anomalies in the central-east and negative ones in the west (purple contours, Figure 2b). This SSH configuration resembles the Kelvin and Rossby wave footprint, representative of the delayed-oscillator mechanism (Battisti 1988; Schopf and Suarez 1988).

The spectrum analysis of these modes reveals that both modes own similar inter-annual peaks (Figure S1c), although HS exhibits larger periodicity (~3.8 years) than the Atlantic Niño (~2.3 years). It implies a higher frequency of occurrence of Atlantic Niño events during the negative AMV period (compared with HS), in agreement with its larger explained variance (Figure 2 and Figure S1). Interestingly, the seasonal evolution of the equatorial temperature tendency denotes a distinct timing for these equatorial modes (Figure 2d). The Atlantic Niño starts to develop in late winter (NDJF) and persists until boreal summer (JJAS, blue line in Figure 2d), while HS pattern illustrates a shorter development, centred in boreal spring (purple line in Figure 2d). The early development and long duration of the Atlantic Niño is a special feature that appears during negative AMV phases and be related to changes in the mean state (Martín-Rey et al. 2018) or the interaction with the boreal winter equatorial variability ('Atlantic Niño II' described by Okumura and Xie (2006)).

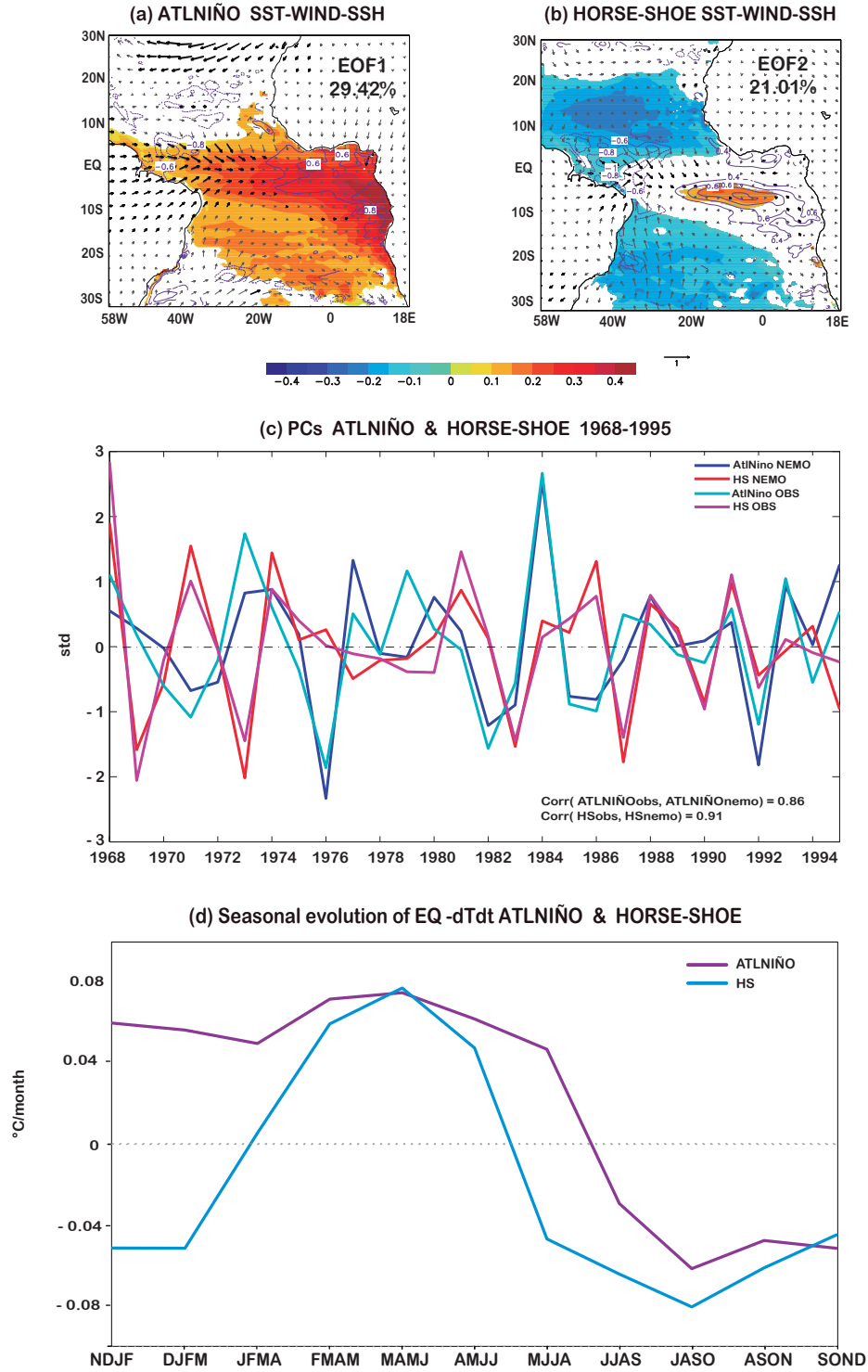


Figure 2. Simulated Atlantic Niño and HS mode. (a-b) Regression maps of anomalous simulated SST (shaded, °C), SSH (contours, cm) and observed surface wind (vectors, m/s) in boreal summer (JJAS) on the PC of the Atlantic Niño (a) and HS (b), also fixed in boreal summer (JJAS). Significant fields exceeding 95% confidence level according to a t-test are presented in shaded, black vectors and purple contours. (c) PCs of Atlantic Niño and HS for the negative AMV period 1968-1995 from model and observations. (d) Time evolution of seasonal temperature tendency in the ML averaged along the equatorial region [30°W-10°E, 5°N-5°S] for Atlantic Niño and HS from boreal winter (NDJF) to fall (SOND).

Our results provide further evidence about the differences between the Atlantic Niño and HS modes, giving robustness to the co-existence of two distinct and independent Equatorial Modes under negative AMV phases (Martín-Rey et al. 2018). It is worth mentioning that, as pointed out by Losada and Rodríguez-Fonseca (2016), the classical Atlantic Niño pattern has also changed during negative AMV periods. We have demonstrated that, in addition to the basin-wide SST configuration, the stronger and westward-shifted equatorial warm tongue, the Atlantic Niño also shows a longer evolution during negative AMV phases (see Figure 5 in Martín-Rey et al. (2018)). All these changes can be understood in terms of a modification in the tropical Atlantic mean state during negative AMV periods. An enhanced thermocline slope could imply an equatorial Atlantic more receptive to wind variations, favouring the activation of diverse ocean dynamics and enhancing the SST variability (Martín-Rey et al. 2018). Under this context, changes in the emergence and timing of the Equatorial Modes under different AMV phases becomes reasonable. Furthermore, a potential interaction between the boreal winter (Okumura and Xie 2006) and summer equatorial Atlantic variability can be also explained the special evolution of the Atlantic Niño during those decades.

The realism of INTER simulation allows us to further investigate the ocean dynamics involved in the development of HS and Atlantic Niño modes. The distribution of their associated SSH anomalies (contours in Figure 2a-b) suggests a possible propagation of oceanic waves. Thus, the wave activity is assessed in next section.

3.2 Wave activity during the Atlantic Niño and Horse-Shoe development

The SSH footprint of HS and Atlantic Niño is also felt in the equatorial Atlantic subsurface, illustrated by thermocline variations (Figure 3a and Figure 4a). The simultaneous alteration of the SSH and thermocline depth suggests the excitation of baroclinic ocean waves. To elucidate the wave activity, time-longitude diagrams of regressed band-pass filtered 5-day SSH and wind stress anomalies onto the time series (PC) of the Atlantic Niño and HS modes are displayed in Figure 3 and Figure 4.

For the Atlantic Niño, the decay of anomalous easterly winds in the western equatorial Atlantic [50°W-40°W] in March originates an anomalous SSH elevation that propagates eastward as a downwelling KW ($dKW1_{AN}$, Figure 3b). The $dKW1_{AN}$ takes one month to reach the African coast (yellow arrow, Figure 3b), consistent with a mix of first and second baroclinic modes ($\sim 1.69\text{m/s}$, Illig et al. (2004)). From April-May, an anomalous wind burst in the western side of the basin triggers a secondary downwelling Kelvin wave, $dKW2_{AN}$ ($\sim 1.13\text{m/s}$), propagating to the east as a mix of second and third baroclinic modes (yellow arrow, Figure 3b). Both dKW s cause deeper thermocline conditions from early spring to late summer (Figure 3a), allowing the Atlantic Niño warming to last up to JJAS (Figure 2a, d).

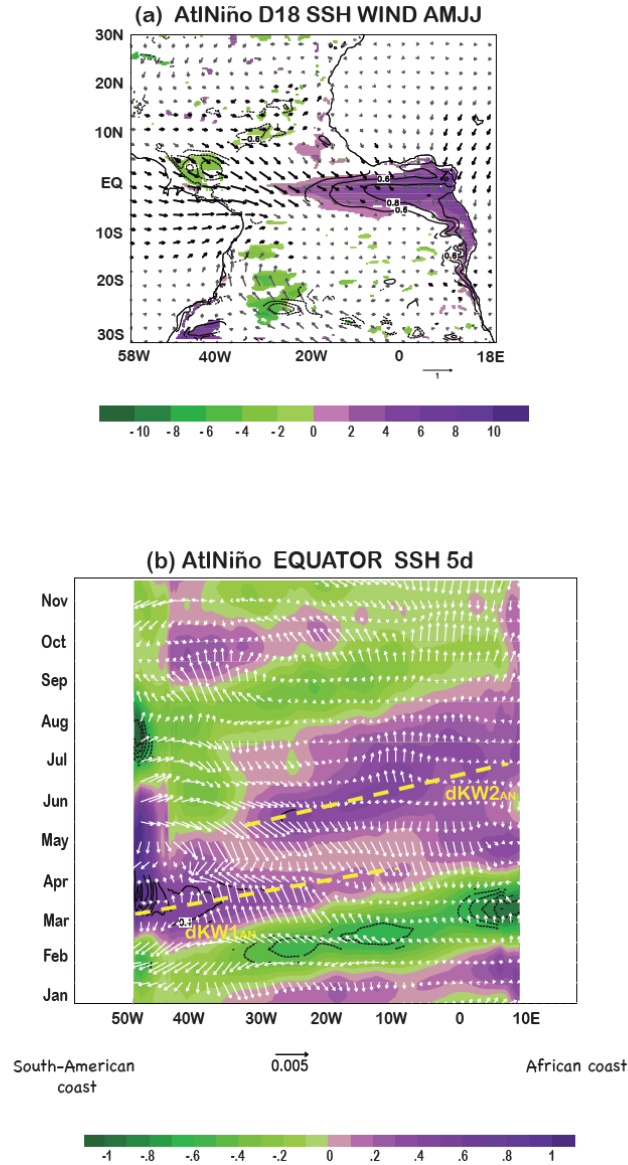


Figure 3. Wave activity involved in the development of Atlantic Niño. (a) Regression of the anomalous observed surface wind (vectors, m/s), thermocline depth (shaded, m) and SSH (contour, cm) in AMJJ onto the PC of Atlantic Niño fixed during boreal summer (JJAS). Significant values exceeding 95% confidence level according to a t-test are shown in shaded, black contours and vectors. (b) Time-longitude diagrams at the equator of the regressed 5-day SSH anomalies (shaded, cm) and wind stress (vectors, N/m^2) from January to December onto the PC of Atlantic Niño. Significant values exceeding 95% according to a t-test are shown in black contours. Downwelling KW are indicated by yellow arrows.

Our results corroborate the existence of Kelvin wave activity during the development of the Atlantic Niño, as proposed in previous studies (Carton and Huang 1994; Hormann and Brandt 2009; Lübbecke et al. 2010). Moreover, we demonstrate that a continuous Kelvin wave propagation occurs from spring to summer months (Figure 3b), preconditioning the equatorial band to generate strong and long Atlantic Niño events during negative AMV phases (Figure 2d and Figure 5 in Martín-Rey et al. (2018)). This has been confirmed using composite analysis (Figure S2a) and individual events (Figure S3). Moreover, our findings highlight the key role of ocean wave propagation in the generation of equatorial variability, in contrast with Nnamchi et al. (2015); (2016).

Noticeably, the development of the HS mode entails more complex wave activity than the Atlantic Niño (Figure 4). An anomalous wind burst in the western equatorial Atlantic [50°W-30°W] in April-May excites a dKW_{HS} , propagating as a mixed of first and second baroclinic mode (~ 1.9 m/s) and reaching the African coast in June (yellow arrow, Figure 4c). As the dKW_{HS} displaces to the east, the SSH elevates and the thermocline deepens (Figure 4a), favouring the development of the warm tongue (Figure 2b). The dKW is reflected in the African coast, returning as an off-equatorial Rossby wave (yellow arrow, Figure 4d). Interestingly, the wave activity in HS mode is not restricted to the local excitation of equatorial Kelvin waves. The basin-scale wind stress field illustrates intensified north-easterlies in NTA contrasting with westerly winds along the equatorial band during boreal spring (purple vectors, Figure 4b). Consequently, an anomalous positive wind stress curl appears north of the equator, associated with a downward Ekman velocity (shaded, Figure 4b) that reduces the SSH in MAMJ (Figure 4d). This negative SSH perturbation at 10°W-20°W propagates to the west as an upwelling RW (uRW_{HS}) from March- to July (blue arrow, Figure 4d), resembling a mix between second and third baroclinic modes (~ 0.31 m/s). The uRW_{HS} is reflected at the western boundary in June, becoming an equatorial $uKW1_{HS}$ (~ 2.33 m/s, mix between first and second baroclinic modes; Figure 4e). The equatorial propagation of $uKW1_{HS}$ rises the thermocline in June-July, allowing for the equatorial cooling (blue arrow, Figure 4e). This remotely-excited $uKW1_{HS}$ acts as a negative feedback, causing the early termination of the equatorial warming, and thus, the HS mode in boreal summer (Figure 2b,d). Notice that, a secondary $uKW2_{HS}$ is triggered from August by anomalous local easterly winds in the western equatorial Atlantic (blue arrow, Figure 4e). The $uKW2_{HS}$ supports the shallower thermocline conditions created by $uKW1_{HS}$, maintaining the favourable scenario for the surface cooling and also contributing to the damping of the HS mode (Figure 2b,d). Additional calculations based on composite analysis (Figure S2c-d) and individual events (Figure S4) confirm the key role of locally and remotely-excited oceanic waves in the development and decay of the HS mode. It is worth mentioning that the RW-reflected mechanism is clearer illustrated in individual HS events (Figure S4) than in the composite map (Figure S2b-c) and regression analysis (Figure 4c-d). The RW-reflected mechanism is found in all HS events, although several discrepancies are shown in the ocean wave activity at the equator, being more active during certain years (i.e: 1981). Additional local forcing, as anomalous wind burst in the western equatorial Atlantic can also trigger equatorial KW that propagate eastward impacting in the SST anomalies, as described for the Atlantic Niño events (Figure S2). Despite the expected differences, the coherent results across diverse methodologies (i.e: regression maps, composites and individual events) give robustness to the existence of the RW-mechanism during the HS mode.

Our results demonstrate the importance of ocean waves in shaping the structure and timing of the Equatorial Modes. Indeed, they play a crucial role in the shorter development of the HS pattern (Figure 4d-e). This RW-reflected mechanism was previously reported as part of the interaction between the Meridional Mode (MM) and the Atlantic Niño pattern (Foltz and McPhaden 2010a, 2010b). Foltz and McPhaden

(2010a) first identified the RW-reflected mechanism during the development of the Meridional Mode acting as a negative delayed feedback for the generation of an Atlantic Niño event during the following summer. Similar results were reported by Lübbecke and McPhaden (2012) associated with the ENSO forcing over the tropical Atlantic variability. These authors suggested that the RW-reflected mechanism is responsible for the inconsistent equatorial Atlantic response to previous winter ENSO.

In addition, with those studies, recent findings have demonstrated that the RW-reflected mechanism has a substantial contribution in generating equatorial SST variability during summer months (Burmeister et al. 2016; Martín-Rey and Lazar 2019). Martín-Rey and Lazar (2019) reveal that during the MM development, a competition between two counteracting effects is established in the equatorial Atlantic: the RW-reflected mechanism and the local wind forcing. Changes in the strength and persistence of each forcing will determine the boreal summer equatorial SST anomalies following a Meridional Mode event (Burmeister et al. 2016; Martín-Rey and Lazar 2019).

In summary, our results bring to light the ocean waves as a key element to modulate the distinct Atlantic Equatorial Modes. In particular, the propagation of locally and remotely excited ocean waves determine the equatorial vertical stratification, which shapes the timing of the Equatorial Modes during negative AMV phases.

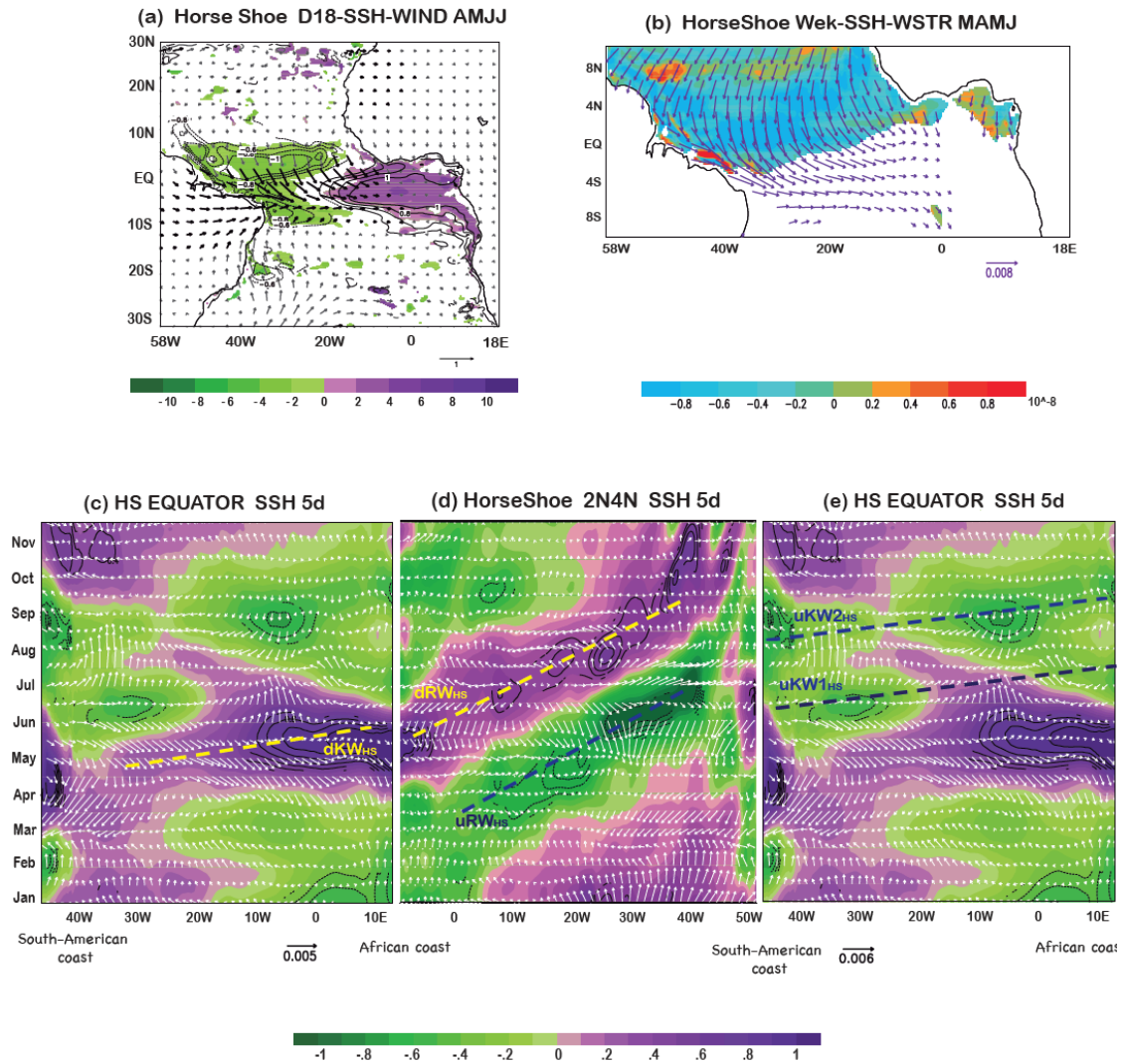


Figure 4. Wave activity involved in the development of HS. (a) Regression of the anomalous observed surface wind (vectors, m/s), thermocline depth (shaded, m) and SSH (contour, cm) in AMJJ onto the PC of the HS fixed during boreal summer (JJAS). Significant values exceeding 95% confidence level according to a t-test are shown in shaded, black and purple contours and vectors. (b) Regressed wind stress (vectors, N/m^2) and wind stress curl (shaded, N/m^3) in MAMJ onto the PC of HS fixed in boreal summer (JJAS). Significant values are shown in shaded, black contours and purple vectors. (c-e) Time-longitude diagrams at the equator (c,e) and 2°N - 4°N (d) of the regressed 5-day SSH anomalies (shaded, cm) and wind stress (vectors, N/m^2) from January to December onto the PC of HS. Significant values exceeding 95% according to a t-test are shown in black contours. Downwelling (upwelling) KW and RW are indicated by yellow (blue) arrows.

3.3 Air-sea interactions in the Atlantic Niño and HS development

INTER reproduces quite well the observed TAV (Figure 2 and S1), providing a reliable ocean simulation to explore the ocean dynamics. To achieve a comprehensive understanding of the associated air-sea processes of Atlantic Niño and HS, a closed heat

budget analysis is carried out from previous winter to spring-summer months with INTER simulation.

3.3.1 Heat Budget analysis of Atlantic Niño mode

For the positive phase of the simulated Atlantic Niño, weakened south-easterlies during previous winter reduce the evaporative heat loss, warming the underneath region (Figure 5a-b). In Angola-Benguela area, anomalous temperature advection by horizontal mean currents generates the surface warming (Figure 5c). In addition, anomalous along-shore winds blowing southward produce an anomalous eastward Ekman transport, inhibiting the upwelling and warming the coastal region (Figure 5d). Notice that the model exhibits an underestimation of the Angola current, with enhanced mean westward currents in the Angola-Benguela area (not shown). This can originate an overestimation of the horizontal advection contribution in this area during the development of the Atlantic Niño. The propagation of coastal Kelvin waves remotely forced at the equator can be responsible of a large part of Angola-Benguela SST variability (Florenchie et al. 2003; Rouault et al. 2007; Polo et al. 2008b; Lübbecke et al. 2010; Rouault et al. 2018). Anomalous SSH anomalies appear along south African coast in April-May (not shown), coherent with the coastal propagation of dKW_{HS} and dKW_{AN} waves. This gives robustness to the importance of ocean waves to generate SST anomalies in Angola-Benguela region. A recent study has proposed air-sea fluxes and river discharge as additional sources for Angola-Benguela SST variability (Lübbecke et al. 2019).

Along the equator, weakened trades during boreal spring trigger a sequence of dKW s that propagate eastward from March to June (Figure 3b), deepening the thermocline (Figure 3a). It allows the activation of vertical diffusion that warms up the equatorial band (Figure 5d,h). These SSTs are advected off-equator and along the south-African coast by horizontal mean currents, shaping the Atlantic Niño warm tongue (Figure 5c,g). In the eastern equatorial Atlantic, at both sides of the equator, the reduced evaporation and cloud cover generates a surface warming through radiative and latent heat fluxes (Figure 5b,f). Finally, the SST over the equatorial band is reduced by surface fluxes (not shown).

In summary, INTER indicates that the southwestern lobe of Atlantic Niño pattern is mainly generated by thermodynamic (air-sea fluxes) mechanisms, while dynamical (thermocline and advective) feedbacks, activated by ocean wave propagation, are essential to develop the equatorial SST anomalies.

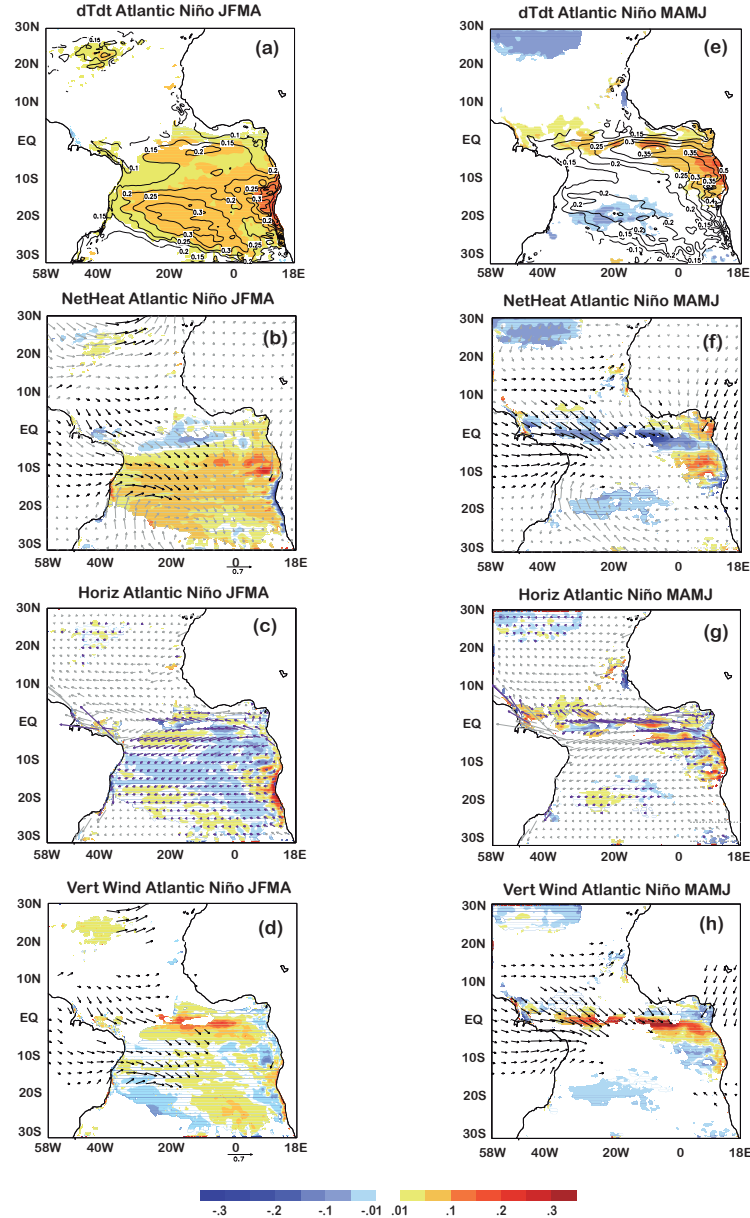


Figure 5. Heat budget analysis for Atlantic Niño. Regression maps of anomalous modeled heat budget terms (in °C/month) in the ML and other variables in JFMA (left) and MAMJ (right) onto the PC of Atlantic Niño fixed in JJAS: (a,e) temperature trend (shaded) and SST (contour, °C); (b,f) net surface heat fluxes (shaded) and surface wind (vectors, m/s); (c,g) horizontal terms (shaded) and mean currents (vectors, m/s); (d,h) vertical terms (shaded) and surface wind (vectors, m/s). Regressions for heat budget terms and mean currents are shown only when temperature tendency regression is significant. Significant fields exceeding 95% confidence level according to a t-test are shown in shaded, black and purple vectors and black contours.

3.3.2 Heat Budget analysis of Horse-Shoe mode

Regarding the simulated HS mode, intensified off-equatorial trades during boreal winter, increase the latent heat loss, cooling the sea surface and developing the HS branches (Figure 6a-b). At the equator, the locally wind-excited dKW_{HS} propagates eastward

during boreal spring (yellow arrow, Figure 4c), deepening the thermocline (Figure 4a) and favouring the surface warming via vertical processes (i.e: vertical diffusion, Figure 6d,h). Horizontal advection illustrates an important contribution south of the equator and along the West-African coast (Figure 6c,g). A significant contribution of surface heat fluxes is also seen in MAMJ in the eastern equatorial warming, at both sides of the equator (Figure 6f).

Interestingly, the excitation of uRW_{HS} , later reflected into uKW_{HS} (Figure 4d-e), provides a negative feedback for the HS mode, causing its early termination in boreal summer (Figure 2d). From June, as uKW_{HS} propagates to the east (Figure 4e), the equatorial thermocline becomes shallower (Figure 4a), allowing the vertical diffusion of deep cold waters and cooling the sea surface (Figure 6i,l). Anomalous temperature advection by horizontal mean currents lead the off-equatorial cold SST anomalies (Figure 6k). This added to the substantial contribution of air-sea fluxes (Figure 6j), damps the HS warm tongue in summer months (Figure 6i and Figure 2d).

Our results from the heat budget analysis, confirm that air-sea fluxes are the main drivers of the HS branches and southwestern lobe of the Atlantic Niño mode. Furthermore, we provide further evidence of the fundamental role of ocean dynamics to generate and modulate the equatorial SST variability (Foltz et al. 2003; Polo et al. 2015a; Dippe et al. 2017; Jouanno et al. 2017). It is noteworthy that both thermocline and advective feedback have a substantial contribution in the development of the Atlantic Niño warm tongue, while thermocline feedback appears as dominant in the generation of the HS pattern. It can be understood by the continuous Kelvin wave propagation, dKW vs uKW , that modify the vertical structure, activating the thermocline feedbacks. Thus, we conclude that wave activity shapes the distinct timing and spatial configuration of the Equatorial Modes during a negative AMV phase.

In the present study, the dynamical nature of the Atlantic Niño has been corroborated for two distinct Equatorial Modes. Ocean dynamics based on vertical diffusion and horizontal advection control the development of equatorial Atlantic SST variability, indicating that thermodynamics are only important for the off-equatorial structure. This disagrees with the results from Nnamchi et al. (2015); (2016), which claimed for the thermodynamic origin of the Atlantic Niño. However, Nnamchi et al. (2015) findings are based on coupled climate models that present a strong bias in their oceanic component (Wang et al. 2014), causing an overestimation of the thermodynamic contribution (Jouanno et al. 2017). On its part, Nnamchi et al. (2016) study of reanalysis datasets is based in an approximated estimation of a not-closed heat budget analysis, in which the air-sea fluxes present a significant but not unique contribution to the mixed layer temperature trend (Nnamchi et al. 2016). Thus, those findings should be interpreted with caution.

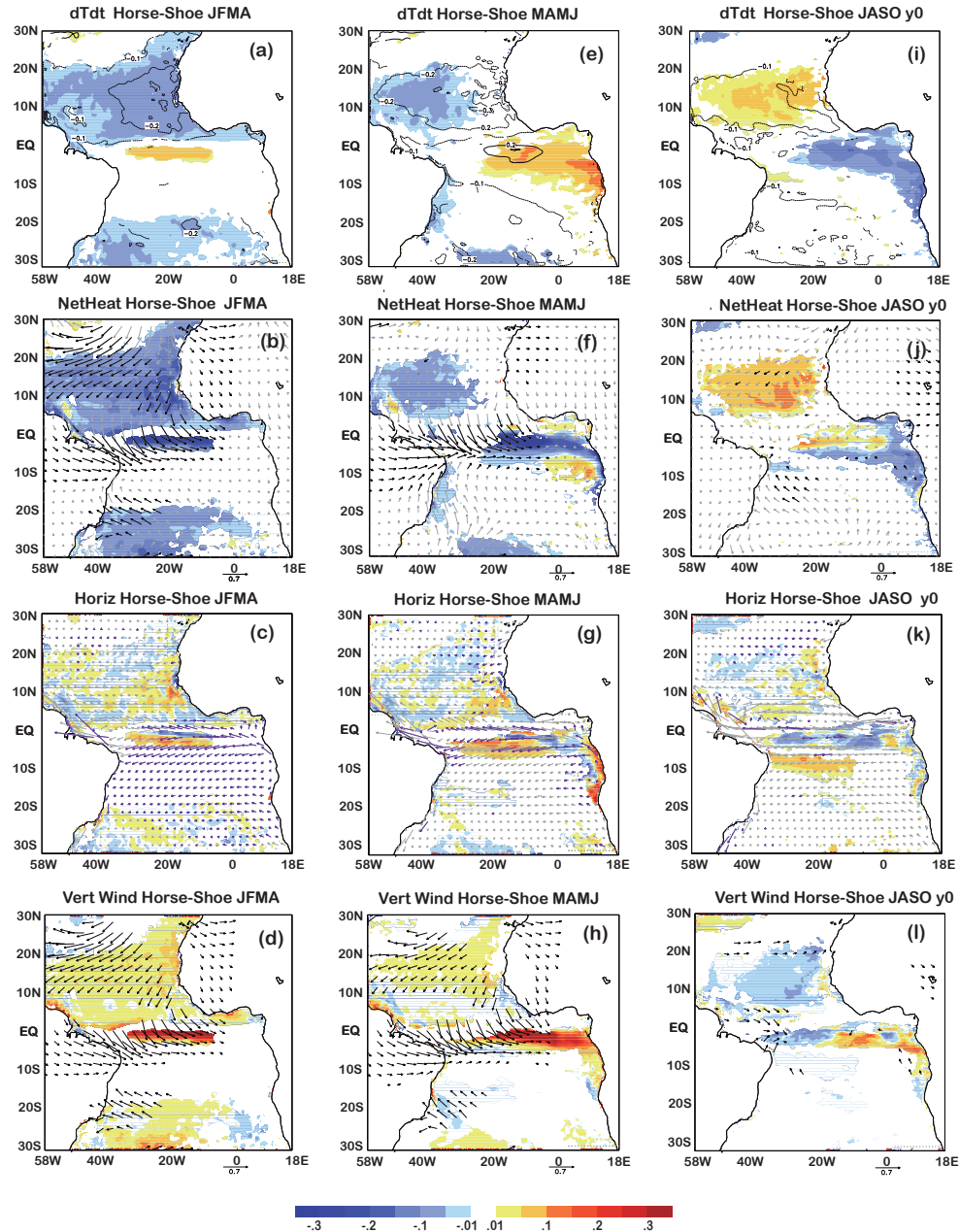


Figure 6. Heat budget analysis for HS. Similar than Figure 5 but for HS mode in JFMA, MAMJ and JASO.

4. Conclusions and Discussion

A previous study revealed the co-existence of two distinct Atlantic Equatorial Modes, the Atlantic Niño and Horse-Shoe, during negative AMV phases (Martín-Rey et al. 2018). During negative AMV, a shallower mean thermocline and enhanced SST in the eastern equatorial Atlantic provides a favourable scenario to investigate the processes that generate the Equatorial Modes. Moreover, the prevailing dynamic view of the Atlantic Niño has been recently questioned and additional mechanisms have been proposed to generate the equatorial Atlantic variability (Brandt et al. 2011; Richter et al. 2013;

Nnamchi et al. 2015, 2016). In this context, a better assessment of the air-sea processes and wave activity responsible to generate the Atlantic Equatorial Modes is necessary.

The present study clarifies the mechanisms underlying the development of the Atlantic Niño and HS mode. For this purpose, we have used an inter-annual forced ocean simulation during a negative AMV period (1968-1995). The main conclusions achieved, illustrated in Figure 7, are enumerated as follows:

- Atlantic Niño and HS modes (amplitude, structure and explained variance) are well reproduced by the model. These two modes represent the inter-annual TAV during the negative AMV period and exhibit different periodicity (~ 3.8 yr for HS and ~ 2.3 yr for the Atlantic Niño).
- For both modes, locally and remotely-excited ocean waves play a fundamental role in the modulation of their distinct structure and timing:
 - a) *Atlantic Niño*: anomalous equatorial westerlies in boreal spring and summer trigger a sequence of downwelling KWs that deepen the thermocline, setting up the favourable conditions to develop and sustain the Atlantic Niño warm tongue.
 - b) *Horse-Shoe mode*: anomalous westerlies in spring excite a dKW_{HS} that reduces the thermocline slope, favouring the warming of the equatorial band. North-equatorial anomalous wind stress curl triggers an uRW_{HS} that propagates westward during boreal spring. The uRW_{HS} is reflected at the western boundary, becoming an upwelling KW_{HS} . The uKW_{HS} acts a negative feedback causing the early termination of the HS mode during boreal summer.
- A closed heat budget analysis has been carried out and the main air-sea processes responsible for Atlantic Niño and HS development have been identified:
 - a) *Atlantic Niño*: air-sea fluxes control the generation of southwestern TA SST anomalies. The decelerated trades diminish the evaporative cooling, warming the sea surface. At the equator, the propagation of the dKW s activates the thermocline and advective feedbacks, responsible to develop the Atlantic Niño warm tongue.
 - b) *Horse-Shoe mode*: intensified northern and southern trades enhance the evaporative heat loss, cooling the sea surface and conforming the horse-shoe branches. At the equator, the propagation of dKW_{HS} during boreal spring decreases the thermocline slope, warming the mixed layer by vertical processes (i.e: vertical diffusion). The remotely-excited uRW_{HS} is western-boundary reflected into uKW_{HS} that causes the thermocline to

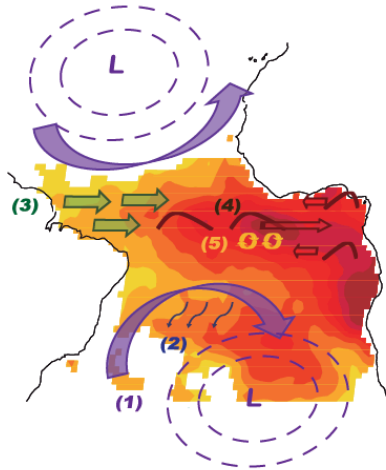
rise, activating the thermocline and advective feedbacks that cool the equatorial band. This uKW_{HS} contributes to damp the initial equatorial warming, causing the early termination of the HS.

Our results give robustness to the importance of ocean dynamics in the development and decay of Equatorial Modes, clarifying its dynamical nature in contrast with the thermodynamic's hypothesis. Especially noteworthy is the important role of the ocean waves baroclinic modes in shaping the distinct structure and timing of Atlantic Niño and HS modes during negative AMV. The RW-reflected mechanism is essential to understand the early termination of the HS mode in boreal summer, and can be key to modulate the connection between the Meridional Mode and Atlantic Niño (Foltz and McPhaden 2010a; Burmeister et al. 2016; Martín-Rey and Lazar 2019).

The present study provides an improvement in the current understanding of TA inter-annual variability and its decadal changes. We have demonstrated, that during negative AMV phases, the enhanced equatorial SST variability due to a favourable mean state contribute to activate diverse ocean dynamics, creating distinct configurations of the Equatorial Mode that co-exist in the tropical Atlantic basin. Figure 7 illustrates that the Atlantic Niño equatorial SST anomalies are mainly generated by thermocline and advective feedbacks (Figure 7a-b), while the enhanced ocean wave activity during HS mode, implies a dominant role of thermocline feedback in the development of the equatorial warm tongue (Figure 7c-d). It is worth mentioning the early beginning (Figure 2d) of the Atlantic Niño mode. This can be favoured by a more receptive tropical Atlantic mean state, but can be also explained by a possible interaction with the so-called 'Atlantic Niño II' peaking in boreal winter (Okumura and Xie 2006). During those decades, the equatorial Atlantic SST variability from previous fall-winter to summer can be connected, originating a longer and more intense Atlantic Niño. This deserves further research that will be carried out by the authors in future studies.

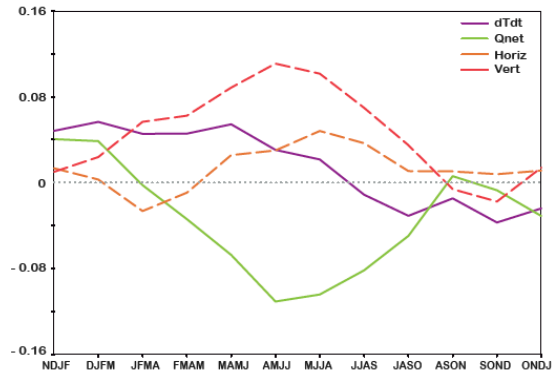
Our findings provide useful information to improve the predictability of the Equatorial Modes. Nevertheless, open questions still remain, aimed to clarify the connection between the Meridional Mode and Equatorial Mode, as well as the contribution of positive AMV background state or Global Warming in the development of TAV. Further research is being carried out by the authors, in the framework of the H2020-EU FESTIVAL project (ref. 797236) to clarify the precursor role of boreal spring variability in generate the equatorial SST anomalies.

(a) Development of Atlantic Niño in AMO neg

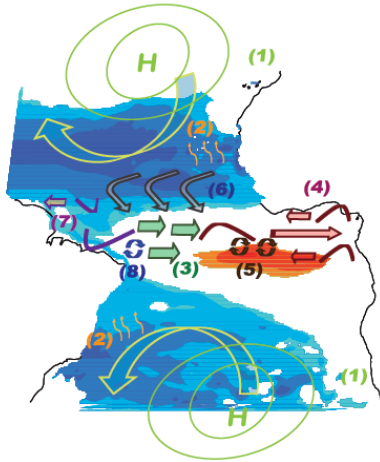


- (1) Weakened Subtropical Highs: reduced trades
- (2) Net heat fluxes warm the STA
- (3) Westerlies along the EQ
- (4) dKW propagating eastward and reflected into dRWs
- (5) Vertical diffusion creates the equatorial warm tongue

(b) HB Atl3 [20W-0,3N-3S] Atlantic Niño



(c) Development of Horse-Shoe in AMO neg



- (1) Strengthened Suptropical Highs, Intensified trades
- (2) Net heat fluxes cool the NTA and STA
- (3) Westerlies along the EQ
- (4) dKW propagates eastward and is reflected into dRW at 5°N and 5°S
- (5) Vertical diffusion creates the equatorial warm tongue
- (6) Cross-equatorial winds create a negative Ekman pumping north of EQ
- (7) uRW at 2°N-5°N is boundary reflected into equatorial uKW
- (8) Vertical diffusion cools the mixed layer, damping the warm tongue

(d) HB Atl3 [20W-0,3N-3S] HS

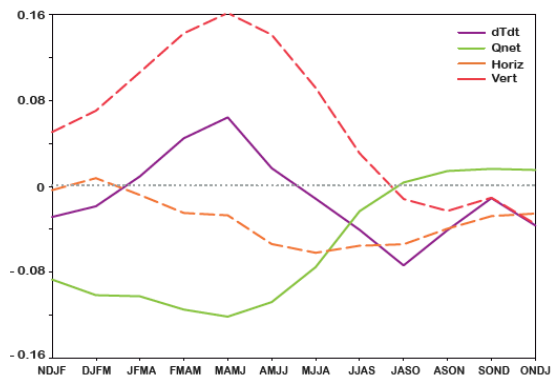


Figure 7. Mechanisms responsible for the development of Atlantic Niño and HS mode. Schematic of the Atlantic Niño (a) and HS (c) development during a negative AMV period. Time evolution of the heat budget terms in the Atl3 [20W-0,3N-3S] region for the Atlantic Niño (b) and HS mode (d) during the negative AMV period 1968-1995.

Acknowledgements: We would like to thank Jean-Marc Molines for his strong support to perform the simulations with the NEMO model. The research leading to these results received funding from the EU FP7/2007-2013 under Grant Agreement 603521 (PREFACE project), the MORDICUS grant under contract ANR-13-SENV-0002-01, the PRE-4CAST (CGL2017-86415-R), CNES/EUMETSAT (CNES - DIA/TEC-2016.8595, EUM/LEO-JAS3/DOC/16/852054), the MSCA-IF-EF-ST FESTIVAL (H2020-EU project 797236) and the EU-TRIATLAS (ref. 817578). The observed SSTs from HadISST dataset were provided by the MetOffice Hadley Centre, from its website at <https://www.metoffice.gov.uk/hadobs/hadisst/>. The data from the INTER simulation are available from the authors upon request.

References

- Battisti, D. S., 1988: Dynamics and thermodynamics of a warming event in a coupled tropical atmosphere-ocean model. *J. Atmos. Sci.*, **45**, 2889-2919.
- Bjerknes, J., 1969: Atmospheric teleconnections from the equatorial Pacific. *Mon. Wea. Rev.*, **97**, 163-172.
- Brandt, P., A. Funk, V. Hormann, M. Dengler, R. J. Greatbatch, and J. M. Toole, 2011: Interannual atmospheric variability forced by the deep equatorial Atlantic Ocean. *Nature*, **473**, 497.
- Brodeau, L., B. Barnier, A. M. Treguier, T. Penduff, and S. Gulev, 2010: An ERA40-based atmospheric forcing for global ocean circulation models. *Ocea. Mod.*, **31**, 88-104.
- Burmeister, K., P. Brandt, and J. Lübbecke, 2016: Revisiting the cause of the eastern equatorial Atlantic cold event in 2009. *J. Geophys. Res.: Oceans*, **121**, 4777-4789.
- Butterworth, S., 1930: On the theory of filter amplifiers. *Experimental wireless and the wireless engineer* **7**, 536-541.
- Carton, J. A., and B. Huang, 1994: Warm Events in the Tropical Atlantic. *J. Phys. Ocea.*, **24**, 888-903.
- de Boyer Montegut, C., G. Madec, A. S. Fischer, A. Lazar, and D. Iudicone, 2004: Mixed layer depth over the global ocean: An examination of profile data and a profile-based climatology. *J. Geophys. Res.: Oceans*, **109**.
- Dippe, T., R. J. Greatbatch, and H. Ding, 2017: On the relationship between Atlantic Niño variability and ocean dynamics. *Clim. Dyn.*
- Faye, S., A. Lazar, B. Sow, and A. Gaye, 2015: A model study of the seasonality of sea surface temperature and circulation in the Atlantic North-eastern Tropical Upwelling System. *FrPhy*, **3**, 76.
- Florenchie, P., J. R. E. Lutjeharms, C. J. C. Reason, S. Masson, and M. Rouault, 2003: The source of Benguela Niños in the South Atlantic Ocean. *Geophys. Res. Lett.*, **30**, 1505.
- Foltz, G. R., and M. J. McPhaden, 2010a: Interaction between the Atlantic meridional and Niño modes. *Geophys. Res. Lett.*, **37**, L18604.
- , 2010b: Abrupt equatorial wave-induced cooling of the Atlantic cold tongue in 2009. *Geophys. Res. Lett.*, **37**, n/a-n/a.
- Foltz, G. R., S. A. Grodsky, J. A. Carton, and M. J. McPhaden, 2003: Seasonal mixed layer heat budget of the tropical Atlantic Ocean. *J. Geophys. Res.: Oceans*, **108**, 3146.
- Goubanova, K., E. Sanchez-Gomez, C. Frauen, and A. Voldoire, 2018: Respective roles of remote and local wind stress forcings in the development of warm SST errors in the South-Eastern Tropical Atlantic in a coupled high-resolution model. *Clim. Dyn.*
- Hormann, V., and P. Brandt, 2009: Upper equatorial Atlantic variability during 2002 and 2005 associated with equatorial Kelvin waves. *J. Geophys. Res.: Oceans*, **114**, C03007.

Illig, S., and Coauthors, 2004: Interannual long equatorial waves in the tropical Atlantic from a high-resolution ocean general circulation model experiment in 1981–2000. *J. Geophys. Res.: Oceans*, **109**, n/a-n/a.

Jouanno, J., O. Hernandez, and E. Sanchez-Gomez, 2017: Equatorial Atlantic interannual variability and its relation to dynamic and thermodynamic processes. *Earth Systems Dynamics*, **8**, 1061-1069.

Keenlyside, N. S., and M. Latif, 2007: Understanding Equatorial Atlantic Interannual Variability. *J. Climate*, **20**, 131-142.

Knight, J. R., C. K. Folland, and A. A. Scaife, 2006: Climate impacts of the Atlantic Multidecadal Oscillation. *Geophys. Res. Lett.*, **33**, L17706.

Kucharski, F., A. Bracco, J. H. Yoo, and F. Molteni, 2008: Atlantic forced component of the Indian monsoon interannual variability. *Geophys. Res. Lett.*, **35**, L04706.

Losada, T., and B. Rodríguez-Fonseca, 2016: Tropical atmospheric response to decadal changes in the Atlantic Equatorial Mode. *Clim. Dyn.*, **47**, 1211-1224.

Losada, T., B. Rodríguez-Fonseca, and F. Kucharski, 2012b: Tropical influence on the summer Mediterranean climate. *AtScL*, **13**, 36-42.

Losada, T., B. Rodríguez-Fonseca, E. Mohino, J. Bader, S. Janicot, and C. R. Mechoso, 2012a: Tropical SST and Sahel rainfall: A non-stationary relationship. *Geophys. Res. Lett.*, **39**, L12705.

Lübbecke, J., and M. J. McPhaden, 2012: On the Inconsistent Relationship between Pacific and Atlantic Niños*. *J. Climate*, **25**, 4294-4303.

———, 2013: A Comparative Stability Analysis of Atlantic and Pacific Niño Modes*. *J. Climate*, **26**, 5965-5980.

Lübbecke, J., C. W. Böning, N. S. Keenlyside, and S.-P. Xie, 2010: On the connection between Benguela and equatorial Atlantic Niños and the role of the South Atlantic Anticyclone. *J. Geophys. Res.: Oceans*, **115**, C09015.

Lübbecke, J., B. Rodríguez-Fonseca, I. Richter, M. Martín-Rey, T. Losada, I. Polo, and N. Keenlyside, 2018: Equatorial Atlantic variability - modes, mechanisms and global teleconnections. *Wiley Interdisciplinary Reviews: Climate Change*.

Lübbecke, J. F., and Coauthors, 2019: Causes and evolution of the southeastern tropical Atlantic warm event in early 2016. *Clim. Dyn.*, **53**, 261-274.

Madec, G., 2008: NEMO ocean engine, Note du Pole de modélisation.

Martín-Rey, M., and A. Lazar, 2019: Is the boreal spring tropical Atlantic variability a precursor of the Equatorial Mode? *Clim. Dyn.*, **53**, 2339-2353.

Martín-Rey, M., B. Rodríguez-Fonseca, I. Polo, and F. Kucharski, 2014: On the Atlantic–Pacific Niños connection: a multidecadal modulated mode. *Clim. Dyn.*, **43**, 3163-3178.

Martín-Rey, M., I. Polo, B. Rodríguez-Fonseca, T. Losada, and A. Lazar, 2018: Is There Evidence of Changes in Tropical Atlantic Variability Modes under AMO Phases in the Observational Record? *J. Climate*, **31**, 515-536.

Nnamchi, H., J. Li, F. Kucharski, I.-S. Kang, N. S. Keenlyside, P. Chang, and R. Farneti, 2015: Thermodynamic controls of the Atlantic Niño. *Nature Communications*, **6**, 8895.

———, 2016: An Equatorial–Extratropical Dipole Structure of the Atlantic Niño. *J. Climate*, **29**, 7295-7311.

North, G. R., T. L. Bell, F. Cahalan, and F. J. Moeng, 1982: Sampling errors in the estimation of empirical orthogonal function. *Mon. Wea. Rev.*, **110** 699–706.

Okumura, Y., and S.-P. Xie, 2006: Some Overlooked Features of Tropical Atlantic Climate Leading to a New Niño-Like Phenomenon*. *J. Climate*, **19**, 5859-5874.

Planton, Y., A. Voldoire, H. Giordani, and G. Caniaux, 2018: Main processes of the Atlantic cold tongue interannual variability. *Clim. Dyn.*, **50**, 1495-1512.

- Polo, I., B. Rodríguez-Fonseca, T. Losada, and J. García-Serrano, 2008a: Tropical Atlantic Variability Modes (1979–2002). Part I: Time-Evolving SST Modes Related to West African Rainfall. *J. Climate*, **21**, 6457–6475.
- Polo, I., A. Lazar, B. Rodríguez-Fonseca, and S. Arnault, 2008b: Oceanic Kelvin waves and tropical Atlantic intraseasonal variability: 1. Kelvin wave characterization. *J. Geophys. Res.: Oceans*, **113**, C07009.
- Polo, I., A. Lazar, B. Rodríguez-Fonseca, and J. Mignot, 2015a: Growth and decay of the equatorial Atlantic SST mode by means of closed heat budget in a coupled general circulation model. *Frontiers in Earth Science*, **3**, 37.
- Rayner, N. A., and Coauthors, 2003: Global analyses of sea surface temperature, sea ice, and night marine air temperature since the late nineteenth century. *J. Geophys. Res.: Atmosphere*, **108**, 4407.
- Richter, I., and S. P. Xie, 2008: On the origin of equatorial Atlantic biases in coupled general circulation models. *Clim. Dyn.*, **31**, 587–598.
- Richter, I., S. K. Behera, Y. Masumoto, B. Taguchi, H. Sasaki, and T. Yamagata, 2013: Multiple causes of interannual sea surface temperature variability in the equatorial Atlantic Ocean. *Nature Geoscience*, **6**, 43–47.
- Richter, I., S. K. Behera, T. Doi, B. Taguchi, Y. Masumoto, and S. P. Xie, 2014: What controls equatorial Atlantic winds in boreal spring? *Clim. Dyn.*, **43**, 3091–3104.
- Rodríguez-Fonseca, B., and Coauthors, 2015: Variability and Predictability of West African Droughts: A Review on the Role of Sea Surface Temperature Anomalies. *J. Climate*, **28**, 4034–4060.
- Rouault, M., S. Illig, J. Lübbecke, and R. A. I. Koungue, 2018: Origin, development and demise of the 2010–2011 Benguela Niño. *J. Mar. Sys.*, **188**, 39–48.
- Rouault, M., S. Illig, C. Bartholomae, C. J. C. Reason, and A. Bentamy, 2007: Propagation and origin of warm anomalies in the Angola Benguela upwelling system in 2001. *J. Mar. Sys.*, **68**, 473–488.
- Schopf, P. S., and M. J. Suarez, 1988: Vacillations in a Coupled Ocean–Atmosphere Model. *J. Atmos. Sci.*, **45**, 549–566.
- Tokinaga, H., and S. Xie, 2011: Weakening of the equatorial Atlantic cold tongue over the past six decades. *Nature Geoscience*, **4**, 222–226.
- Vialard, J., C. Menkes, J.-P. Boulanger, P. Delecluse, E. Guilyardi, M. J. McPhaden, and G. Madec, 2001: A Model Study of Oceanic Mechanisms Affecting Equatorial Pacific Sea Surface Temperature during the 1997–98 El Niño. *J. Phys. Ocea.*, **31**, 1649–1675.
- von Storch, H., and F. Zwiers, 2001: Statistical Analysis in Climate Research. *Cambridge University Press*, 484.
- Wang, C., L. Zhang, S. K. Lee, L. Wu, and C. R. Mechoso, 2014: A global perspective on CMIP5 climate model biases. *Nature Climate Change*, **4**, 201–205.
- Zebiak, S. E., 1993: Air–Sea Interaction in the Equatorial Atlantic Region. *J. Climate*, **6**, 1567–1586.

Figure Caption

Figure 1. Validation of INTER simulation. Bias of the annual SST(a), SSH (b) and thermocline depth (D18, c) of INTER simulation with respect to SODA reanalysis for the period the period 1960–2008.

Figure 2. Simulated Atlantic Niño and HS mode. (a–b) Regression maps of anomalous simulated SST (shaded, °C), SSH (contours, cm) and observed surface wind (vectors,

m/s) in boreal summer (JJAS) on the PC of the Atlantic Niño (a) and HS (b), also fixed in boreal summer (JJAS). Significant fields exceeding 95% confidence level according to a t-test are presented in shaded, black vectors and purple contours. (c) PCs of Atlantic Niño and HS for the negative AMV period 1968-1995 from model and observations. (d) Time evolution of seasonal temperature tendency in the ML averaged along the equatorial region [30°W-10°E, 5°N-5°S] for Atlantic Niño and HS from boreal winter (NDJF) to fall (SOND).

Figure 3. Wave activity involved in the development of Atlantic Niño. (a) Regression of the anomalous observed surface wind (vectors, m/s), thermocline depth (shaded, m) and SSH (contour, cm) in AMJJ onto the PC of Atlantic Niño fixed during boreal summer (JJAS). Significant values exceeding 95% confidence level according to a t-test are shown in shaded, black contours and vectors. (b) Time-longitude diagrams at the equator of the regressed 5-day SSH anomalies (shaded, cm) and wind stress (vectors, N/m²) from January to December onto the PC of Atlantic Niño. Significant values exceeding 95% according to a t-test are shown in black contours. Downwelling KW are indicated by yellow arrows.

Figure 4. Wave activity involved in the development of HS. (a) Regression of the anomalous observed surface wind (vectors, m/s), thermocline depth (shaded, m) and SSH (contour, cm) in AMJJ onto the PC of the HS fixed during boreal summer (JJAS). Significant values exceeding 95% confidence level according to a t-test are shown in shaded, black and purple contours and vectors. (b) Regressed wind stress (vectors, N/m²) and wind stress curl (shaded, N/m³) in MAMJ onto the PC of HS fixed in boreal summer (JJAS). Significant values are shown in shaded, black contours and purple vectors. (c-e) Time-longitude diagrams at the equator (c,e) and 2°N-4°N (d) of the regressed 5-day SSH anomalies (shaded, cm) and wind stress (vectors, N/m²) from January to December onto the PC of HS. Significant values exceeding 95% according to a t-test are shown in black contours. Downwelling (upwelling) KW and RW are indicated by yellow (blue) arrows.

Figure 5. Heat budget analysis for Atlantic Niño. Regression maps of anomalous modelled heat budget terms (in °C/month) in the ML and other variables in JFMA (left) and MAMJ (right) onto the PC of Atlantic Niño fixed in JJAS: (a,e) temperature trend (shaded) and SST (contour, °C); (b,f) net surface heat fluxes (shaded) and surface wind (vectors, m/s); (c,g) horizontal terms (shaded) and mean currents (vectors, m/s); (d,h) vertical terms (shaded) and surface wind (vectors, m/s). Regressions for heat budget terms and mean currents are shown only when temperature tendency regression is significant. Significant fields exceeding 95% confidence level according to a t-test are shown in shaded, black and purple vectors and black contours.

Figure 6. Heat budget analysis for HS. Similar than Figure 5 but for HS mode in JFMA, MAMJ and JASO.

Figure 7. Mechanisms responsible for the development of Atlantic Niño and HS

792 **mode.** Schematic of the Atlantic Niño (a) and HS (c) development during a negative
793 AMV period. Time evolution of the heat budget terms in the Atl3 [20W-0,3N-3S]
794 region for the Atlantic Niño (b) and HS mode (d) during the negative AMV period
795 1968-1995
796
797
798